Progress of Theoretical Physics, Vol. 100, No. 6, December 1998

Semiclassical Origin of Superdeformed Shell Structure in the Spheroidal Cavity Model

Ken-ichiro ARITA, Ayumu SUGITA* and Kenichi MATSUYANAGI*

Department of Physics, Nagoya Institute of Technology, Nagoya 466-8555, Japan
**Department of Physics, Graduate School of Science, Kyoto University*
Kyoto 606-8502, Japan

(Received September 2, 1998)

Classical periodic orbits responsible for emergence of the superdeformed shell structures of single-particle motion in spheroidal cavities are identified and their relative contributions to the shell structures are evaluated. Both prolate and oblate superdeformations (axis ratio approximately 2:1) as well as prolate hyperdeformation (axis ratio approximately 3:1) are investigated. Fourier transforms of quantum spectra clearly show that three-dimensional periodic orbits born out of bifurcations of planar orbits in the equatorial plane become predominant at large prolate deformations, while butterfly-shaped planar orbits bifurcated from linear orbits along the minor axis are important at large oblate deformations.

§1. Introduction

In the last decade, superdeformed spectroscopy, i.e., the study of nuclear structure with large prolate deformations (axis ratio approximately 2:1), has developed enormously, and further significant progress is expected.[1)-3)] It is well known that the superdeformation is the result of shell effect at large deformation, and in fact realistic calculations of both the Strutinsky-Nilsson type and Hartree-Fock type work well for describing shell structures observed in experiments at such large deformations.[4)] The purpose of this paper, however, is not to make some realistic calculations in relation to recent experimental findings. Rather, we address here the fundamental question of why a nucleus is superdeformed and investigate the semiclassical origin of emergence of the superdeformed shell structure in a simple model, a spheroidal cavity model.

In the periodic-orbit theory,[5)-8)] based on the semiclassical approximation of the path integral, oscillating parts of single-particle level densities are determined by periodic orbits in the classical counterpart of the single-particle Hamiltonian. We are particularly interested in shell structure, i.e., level densities coarse-grained to a certain energy resolution, which are related with short periodic orbits. As is well known, a nucleus favors such shapes at which prominent shell structures are formed and its Fermi surface lies in a valley of oscillating level density, increasing its binding energy in this way.

With a semiclassical approach, Strutinsky et al.[9)] studied the shell structure associated with the spheroidal cavity model and found that planar orbits in the meridian plane are responsible for the shell structure at normal prolate deformations. In addition, they pointed out that some three-dimensional (3D) periodic orbits ap-

pearing at large deformations lead to the shell structure responsible for the fission isomers whose existence has been known since the 1970s, which have superdeformed shapes. As emphasized in Ref. 9), shell structures obtained for the spheroidal cavity model contain basic features, apart from shifts of deformed magic numbers due to the spin-orbit potential, similar to those obtained by the Woods-Saxon potential for heavy nuclei and metallic clusters, and thus this model can be used as a simple model to understand the semiclassical origin of the emergence of regular oscillating patterns in the coarse-grained quantum spectra at large deformations.

Remarkably, however, two decades after the publication of Ref. 9), to the best of our knowledge, little exploration of this idea has been undertaken and the qualitative argument given in that paper has not been fully examined by other researchers, although the spheroidal cavity model has been used for various purposes.[10)-12)] A paper most relevant to the present paper is that of Frisk,[13)] who used the periodic-orbit theory and the same cavity model mainly to clarify the origin of the prolate-oblate asymmetry at normal deformations. Although he also briefly discussed the case of large deformations, the importance of 3D orbits was not mentioned.

In this paper, we identify the most important periodic orbits that determine the major pattern of the oscillating level density at large deformations, including prolate superdeformations, prolate hyperdeformations and oblate superdeformations. For this purpose we make full use of the Fourier transformation method. As briefly reviewed in the text, by virtue of the scaling property of the cavity model, Fourier transforms of quantum spectra exhibit peaks at lengths of classical periodic orbits, enabling us to precisely identify important periodic orbits contributing to the shell structure. This method has been well known,[6),8)] but it has not been used for the present subject.

Classical periodic orbits in a spheroidal cavity and their bifurcations with the variation of the axis ratio have been thoroughly studied by Nishioka et al.[14),15)] This paper may be regarded as a continuation of their work in the sense that we investigate quantum manifestations of these periodic orbits and of their bifurcations. (Actually, this was the intention also of the work by Nishioka et al.[14),15)])

We present in §2 the oscillating parts of smoothed level densities as functions of the deformation parameter of the cavity. The Fourier transformation method is recapitulated in §3. Periodic orbits and their bifurcations in a spheroidal cavity are briefly reviewed in §4. The results of the semiclassical analysis of shell structures are presented in §§6–8 for prolate superdeformations, prolate hyperdeformations and oblate superdeformations, respectively, and conclusions are given in §9.

A part of this work was previously reported in conference proceedings.[16)]

§2. Oscillating level density

We solve the Schrödinger equation for single-particle motion in a spheroidal cavity under Dirichlet boundary conditions. As is well known, a spheroidal cavity model is integrable and separable by the spheroidal coordinate system, so that these coordinates are frequently used for solving the Schrödinger equation. We have, however, adopted a spherical-wave decomposition method[17)] for this purpose. The

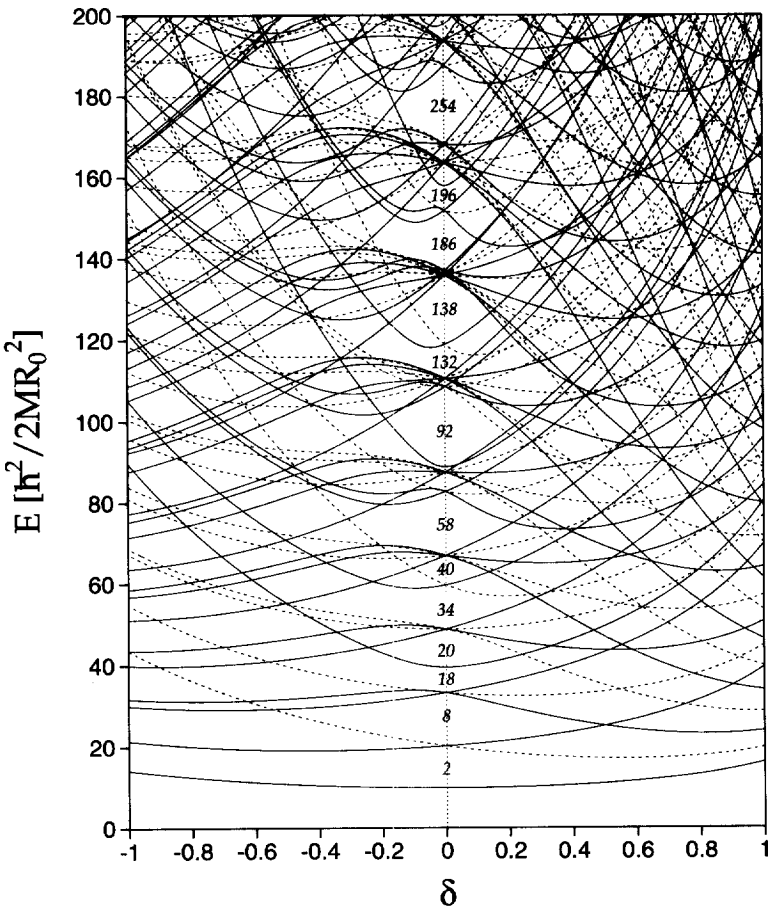

Fig. 1. Single-particle energy diagram for a spheroidal cavity, plotted as a function of the deformation parameter δ. Solid and broken lines represent even- and odd-parity levels. The energy is measured in units of $\hbar^2/2MR_0^2$, where M and R_0 are the mass of the particle and the radius in the spherical limit, respectively. The spin degeneracy factor 2 is taken into account in magic numbers in the spherical limit.

reason is merely that we wrote a computer program based on the latter method for the purpose of efficiently calculating a large number of eigenvalues as function of deformation parameters for cavities of general axially symmetric shapes.[18] With this method, wave functions are expanded in terms of spherical Bessel functions (for the radial coordinate) and associated Legendre functions (for the polar angle coordinate), and expansion coefficients are determined so as to fulfill the boundary conditions (see Refs. 18) and 17) for technical details).

The single-particle energy diagram (as function of deformation parameter δ) obtained in this way is shown in Fig. 1. The deformation parameter δ is related to the axis ratio $\eta \equiv a/b$ by $\delta = 3(\eta - 1)/(2\eta + 1)$ in the prolate case and by $\delta = -3(\eta - 1)/(\eta + 2)$ in the oblate case, where a and b denote the lengths of the major and the minor axes, respectively. The volume-conservation condition is

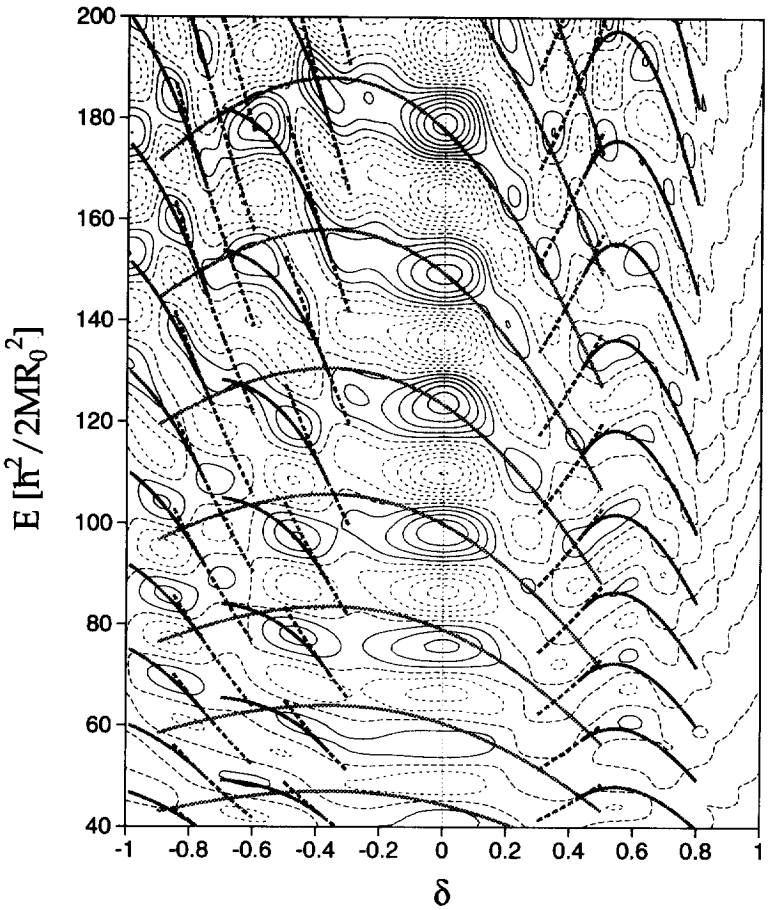

Fig. 2. Oscillating part of the smoothed level density displayed as a function of the energy and deformation parameter δ. Solid, dashed and dotted contour curves correspond to negative, zero and positive values, respectively. The units of energy are the same as in Fig. 1. Strutinsky smoothing is used, with the smoothing width parameter $\Delta k = 0.5$. Constant-action lines for important periodic orbits are indicated: Thick solid lines running through the spherical closed shells are those for tetragonal orbits in the meridian plane. Thick broken and solid lines in the region $\delta = 0.3 \sim 0.8$ are those for five-point star-shaped orbits in the equatorial plane and for 3D orbits (5:2:1) bifurcated from them, respectively. Broken and solid lines in the region $\delta = -0.3 \sim -0.7$ are those for double repetitions of linear orbits along the minor axis and for butterfly-shaped planar orbits (4:1:1) bifurcated from them, respectively. Similarly, broken and solid lines in the region $\delta = -0.6 \sim -1$ are those for triple repetitions of linear orbits along the minor axis and for planar orbits (6:1:1) bifurcated from them, respectively.

imposed so that $ab^2 = R_0^3$ in the prolate case and $a^2b = R_0^3$ in the oblate case, where R_0 is the radius in the spherical limit.

Figures 2 and 3 display the oscillating part of the smoothed level density in the form of a contour map with respect to the energy and deformation parameter, which is coarse-grained with the Strutinsky smoothing parameter $\Delta k = 0.5$. We clearly see regular patterns consisting of several valley and ridge structures. Thick solid and

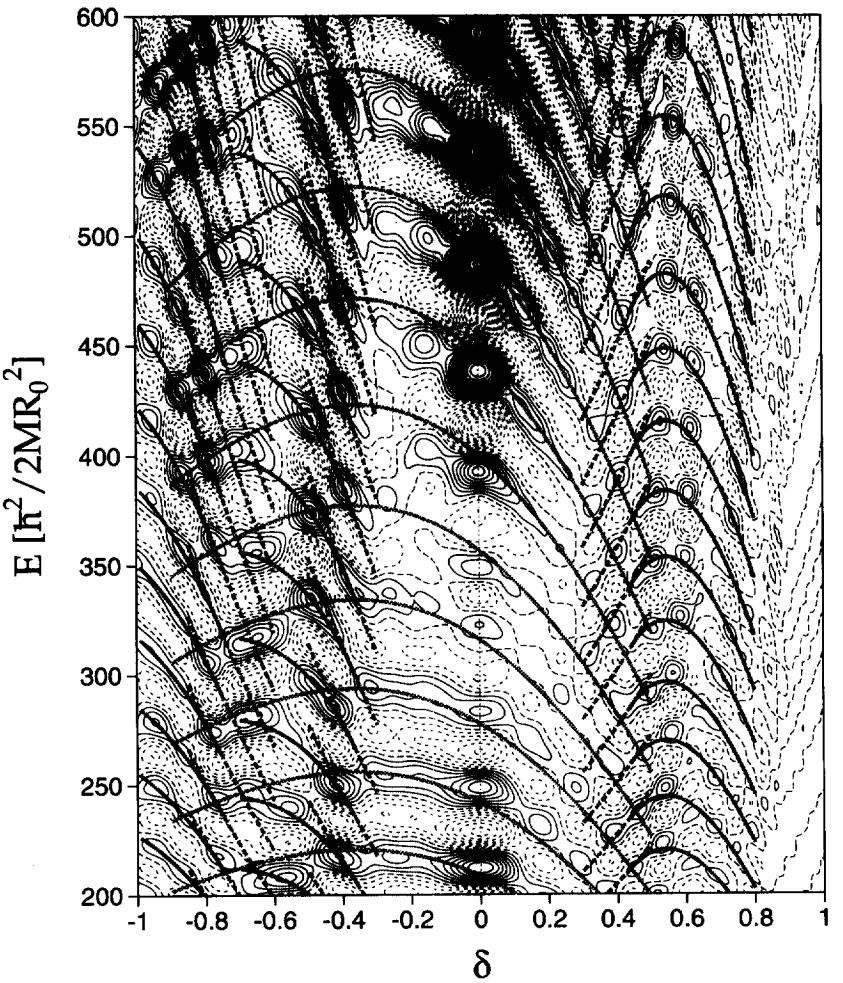

Fig. 3. Same as Fig. 2 but for a higher energy region. The correspondence between valley structures and constant-action curves becomes much clearer in the higher energy region.

broken lines indicate the valley lines predicted by the periodic orbit theory (see §5 and §§6–8 for details).

§3. Fourier transform

Single-particle equations of motion for the cavity are invariant with respect to the scaling transformation $(\boldsymbol{x}, \boldsymbol{p}, t) \rightarrow (\boldsymbol{x}, \alpha\boldsymbol{p}, \alpha^{-1}t)$ and the action integral S_r for a periodic orbit r is proportional to its length L_r:

$$S_r(E = p^2/2M) = \oint_r \boldsymbol{p} \cdot d\boldsymbol{q} = pL_r = \hbar k L_r. \tag{3·1}$$

Thus the semiclassical trace formula for the level density [5] is written as

$$g(E) = \sum_n \delta(E - E_n) = \frac{M}{\hbar^2 k} \sum_n \delta(k - k_n)$$
$$\simeq \bar{g}(E) + \sum_r A_r(k) \cos(kL_r - \pi\mu_r/2), \tag{3·2}$$

where $\bar{g}(E)$ denotes the smooth part corresponding to the contribution of the *zero-length* orbit, and μ_r is the Maslov phase of the periodic orbit r. This scaling property enables us to make use of the Fourier transformation of the level density with respect to the wave number k. The Fourier transform $F(L)$ of the level density $g(E)$ is written as

$$F(L) = \int dk\, e^{-ikL} g(E = \hbar^2 k^2/2M)$$
$$\simeq \bar{F}(L) + \pi \sum_r e^{-i\pi\mu_r/2} A_r(i\partial_L)\, \delta(L - L_r), \tag{3·3}$$

which may be regarded as the 'length spectrum' exhibiting peaks at lengths of individual periodic orbits. [6] In numerical calculations, the spectrum is cut off by a Gaussian with cutoff wave number $k_c = 1/\Delta L$ as

$$F_{\Delta L}(L) \equiv \frac{1}{\sqrt{2\pi}\Delta L} \int dL'\, e^{-\frac{1}{2}(\frac{L-L'}{\Delta L})^2} F(L')$$
$$= \frac{M}{\hbar^2} \sum_n \frac{1}{k_n} e^{-\frac{1}{2}(k_n/k_c)^2} e^{-ik_n L}, \tag{3·4}$$
$$\simeq \bar{F}_{\Delta L}(L) + \pi \sum_r e^{-i\pi\mu_r/2} A_r(i\partial_L) \frac{1}{\sqrt{2\pi}\Delta L} e^{-\frac{1}{2}(\frac{L-L_r}{\Delta L})^2}. \tag{3·5}$$

§4. Periodic-orbit bifurcations

In this section, we recapitulate the theory of classical periodic orbits in the spheroidal cavity following Nishioka et al. [14),15)] and Strutinsky et al. [9)] We focus our attention on those orbits having short periods.

As is well known, only linear and planar orbits exist in a spherical cavity. When spheroidal deformations appear, the linear (diameter) orbits bifurcate into those along the major axis and along the minor axis. Likewise, the planar orbits bifurcate into orbits in the meridian plane and those in the equatorial plane. Since the spheroidal cavity model is integrable, all classical orbits lie on a 3D torus, and, in the case of a prolate spheroid, periodic orbits are characterized by three positive integers (p:t:q), which represent numbers of vibrations or rotations with respect to three spheroidal coordinates. They are denoted as $(n_\epsilon, n_\phi, n_\xi)$ in Refs. 14) and 15), and (n_v, n_ϕ, n_u) in Ref. 9). When the axis ratio η of the prolate spheroid increases, hyperbolic orbits in the meridian plane and three-dimensional orbits successively appear through bifurcations of linear and planar orbits in the equatorial plane. Bifurcations occur when the condition

$$\eta \equiv \frac{a}{b} = \frac{\sin(\pi t/p)}{\sin(\pi q/p)} \tag{4·1}$$

is satisfied.

As we see in succeeding sections, the most important orbits for superdeformed shapes (axis ratio approximately 2:1) are 3D orbits $(p{:}t{:}q) = (p{:}2{:}1)$ with $p = 5, 6, 7, \cdots$. They bifurcate from planar orbits that turn twice ($t = 2$) about the symmetry axis. Likewise, planar orbits (4:2:1) bifurcate from linear orbits that repeat twice along the minor axis. These new-born orbits resemble the Lissajous figures of the superdeformed harmonic oscillator with frequency ratio $\omega_\perp{:}\omega_z = 2{:}1$. Every bifurcated orbit forms a continuous family of degeneracy two, which implies that we need two parameters to specify a single orbit among a continuous set of orbits belonging to a family having a common value of the action integral (or equivalently, the length).

For prolate hyperdeformed shapes (axis ratio approximately 3:1), bifurcations from linear and planar orbits that turn three times ($t = 3$) about the symmetry axis are important. The new-born orbits are hyperbolic orbits in the meridian plane (6:3:1) and 3D orbits $(p{:}3{:}1)$ with $p = 7, 8, 9, \cdots$.

In the case of oblate spheroidal cavities, periodic orbits are classified in Ref. 15) into two modes, the whispering-gallery (W) mode and bouncing-ball (B) mode. The systematics of periodic-orbit bifurcations for the W-mode are similar to those for the prolate case and can be treated by just exchanging the roles of t and q. On the other hand, B-mode orbits are successively created through bifurcations of multiple repetitions of linear orbits along the minor axis when the condition

$$\eta \equiv \frac{a}{b} = \frac{1}{\sin(\pi t/p)} \tag{4·2}$$

is satisfied. Bifurcations of this kind do not depend on q, so that, for instance, planar orbits (4:1:1) are created simultaneously with two families of 3D orbits (4:1:3/2) and (4:1:2). (For B-mode orbits, half integer values of q are allowed as well as integers, due to different definitions of the integration range for the action integral related to q; see Ref. 15).)

Bifurcation points and variations of lengths with deformation are displayed for some short periodic orbits in Table I and Fig. 4.

Table I. Bifurcation points of periodic orbits specified by $(p{:}t{:}q)$ in the spheroidal cavity. Only those for short orbits to be discussed in §§6–8 are displayed.

orbit $(p{:}t{:}q)$	axis ratio (a/b)	deformation δ	orbit length in R_0
(4:2:1)	1.414	0.325	7.127
(5:2:1)	1.618	0.438	8.101
(6:2:1)	1.732	0.492	8.654
(7:2:1)	1.802	0.523	8.995
(8:2:1)	1.848	0.542	9.220
(6:3:1)	2.0	0.6	9.524
(7:3:1)	2.247	0.681	10.421
(8:3:1)	2.414	0.728	11.011
(9:3:1)	2.532	0.758	11.437
(4:1:1)	1.414	−0.364	6.350
(6:1:1)	2.0	−0.75	7.560

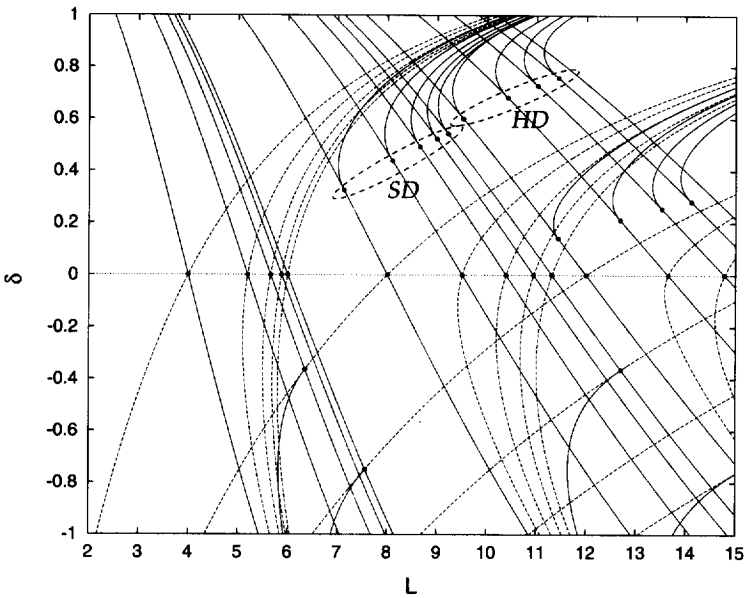

Fig. 4. Variations of lengths of periodic orbits in a spheroidal cavity with respect to the deformation parameter δ. Only those for short orbits discussed in §§6–8 are displayed. For a more complete diagram, see Nishioka et al.[14),15)]

§5. Shell structure and constant-action line

Using the trace formula, we can extract information about classical periodic orbits from the Fourier transforms of the level density. In this section we discuss another method of using the trace formula, the constant-action line analysis.[9)] As stated in §3 (see Eq. (3·2)), the quantum level density can be represented as the summation over periodic orbits. If a few orbits having nearly the same action integral dominate in the sum, it is expected that valleys in the contour map of the oscillating part of the smoothed level density versus energy E and deformation δ will be characterized by constant-action lines $S(E,\delta) = \text{const}$ for those dominant orbits. The equation for such lines is $kL_r(\delta) - \pi\mu_r/2 = (2n+1)\pi$, thus,

$$E(\delta) = \frac{1}{2M}\left(\frac{2\pi\hbar(n+1/2+\mu_r/4)}{L_r(\delta)}\right)^2. \quad (n=0,1,2,\cdots) \tag{5·1}$$

As an example, let us examine the shell structure at normal deformations $|\delta| \lesssim 0.3$. In this region, triangular and tetragonal orbits in the meridian plane give dominant contributions to the level density. This fact was first pointed out by Strutinsky et al.[9)] (Although the triangular orbits were overlooked there, actions of the two families of orbits scale in the same way as functions of deformation parameter so that their argument was correct in essence.) The Fourier amplitudes at lengths of some meridian-plane orbits are plotted in Fig. 5 as functions of the deformation parameter δ. We see that the meridian-plane orbits are important for small δ and that their contributions decline with increasing $|\delta|$. In Figs. 2 and 3, constant-

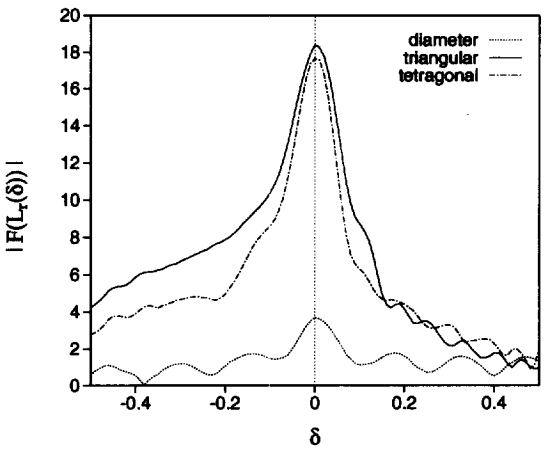

Fig. 5. Absolute values of the Fourier amplitudes defined in Eq. (3·4), at lengths $L = L_\tau$ of some short meridian-plane orbits, plotted as functions of the deformation parameter δ.

action lines (5·1) for the tetragonal orbits in the meridian plane are indicated. The period of the shell oscillation is mainly determined by the tetragonal orbits, and the valley structure of the level density at normal deformation is nicely explained by their constant-action lines. We also note that the shell effect at spherical shape is weakened at $E \sim 300$, and the phase of valley is shifted from that of the constant-action lines for $E \simeq 250$–350. This is due to the supershell effect associated with the interference of the triangular and tetragonal orbits.[6),19)]

In this way, we can analyze the properties of the shell structure through classical periodic orbits. In the following sections, we utilize these techniques in order to identify dominant classical periodic orbits that characterize the shell structures in superdeformed shapes.

§6. Prolate superdeformations

Figure 6 displays Fourier transforms of quantum spectra for prolate spheroidal cavities with deformation parameter values $\delta = 0.1 \sim 0.6$. At normal deformations with $\delta = 0.1$, as mentioned in the previous section, we notice peaks associated with triangular and tetragonal orbits in the meridian plane. With increasing deformation, bifurcations of linear and planar orbits in the equatorial plane successively take place. Thus, the highest peak at $L \simeq 7$ of the Fourier transform for $\delta = 0.4$ is associated with butterfly-shaped planar orbits $(p{:}t{:}q) = (4{:}2{:}1)$ that bifurcate at $\delta \simeq 0.32$ from double repetitions of linear orbits along the minor axis. For $\delta = 0.5$, the prominent peaks at $L \simeq 8$ and 8.6 correspond to 3D orbits (5:2:1) and (6:2:1) bifurcated respectively from five-point star-shaped orbits and double traversals of triangular orbits in the equatorial plane. With further increase in δ, the same kind of 3D orbits successively bifurcate from equatorial-plane orbits. For $\delta = 0.6$ (axis ratio $\eta = 2$), peaks around $L \simeq 9$ are associated with 3D orbits (7:2:1) and (8:2:1) that are bifurcated from 7-point star-shaped orbits and double traversals of rectangular orbits in the equatorial

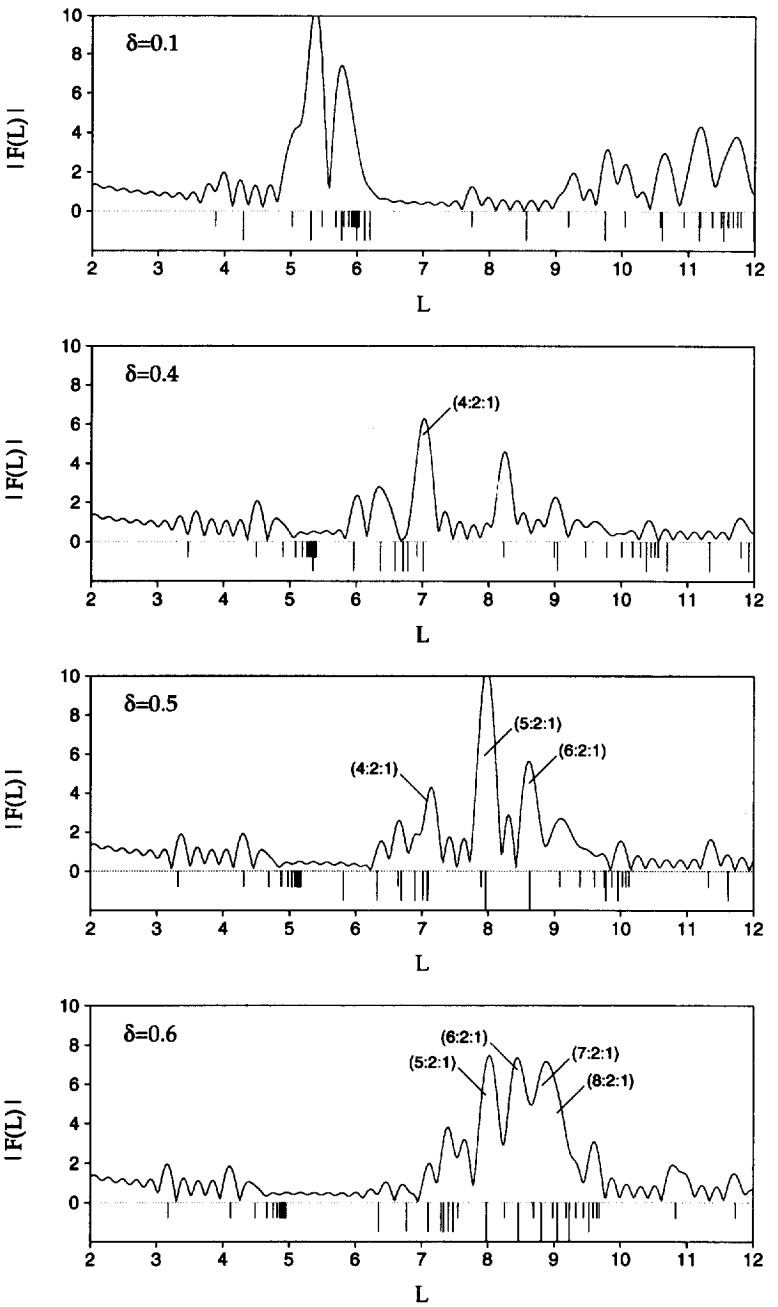

Fig. 6. Length spectra (Fourier transforms of quantum level densities) for spheroidal cavities with deformation parameter $\delta = 0.1, 0.4, 0.5$ and 0.6. The cutoff wave number $k_c = \sqrt{600}$ is used in Eq. (3·4). At the bottom of each figure, the lengths of classical periodic orbits are indicated by vertical lines. Long, middle and short vertical lines are used for 3D orbits, planar orbits in the meridian, and planer orbits in the equatorial planes, respectively.

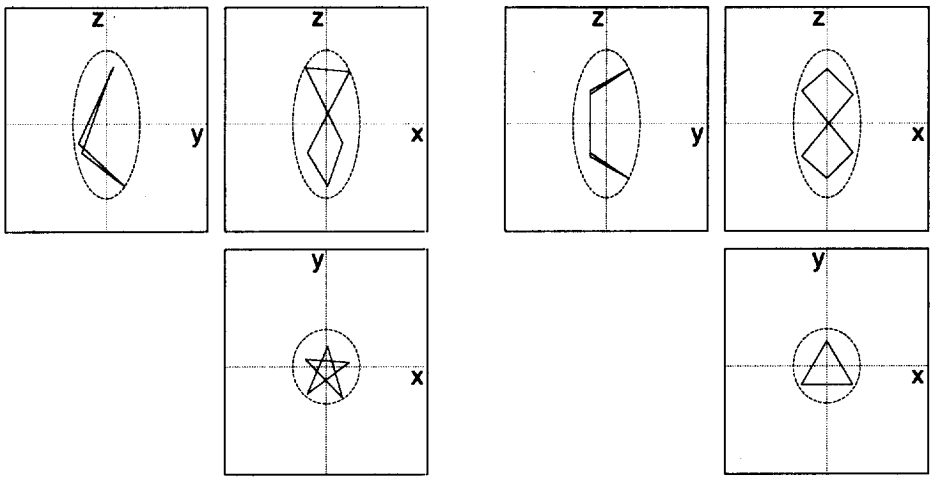

Fig. 7. Three-dimensional orbits (5:2:1) and (6:2:1) in the superdeformed prolate cavity with deformation $\delta = 0.6$ (axis ratio $\eta = 2$). Their projections on the (x, y), (y, z) and (z, x) planes are displayed.

plane.

In Figs. 2 and 3, constant-action lines for the 3D orbits (5:2:1) are indicated. Good correspondence is found between these lines and the valley structure seen in the superdeformed region with δ around 0.6. Thus we can conclude that the bifurcations of equatorial orbits play essential roles in the formation of the superdeformed shell structure, and this shell structure is characterized by the 3D orbits (p:2:1).

Some of these 3D orbits are displayed in Fig. 7. They possess similarities with the figure-eight shaped orbits in the superdeformed harmonic oscillator with frequency ratio $\omega_\perp{:}\omega_z = 2{:}1$. An important difference between the cavity model under consideration and the harmonic oscillator model should be noted, however: In the former, such periodic orbits exist for all deformation parameters δ larger than the bifurcation points, whereas in the latter, such orbits appear only for special deformations corresponding to rational ratios of the major and minor axes.

On the other hand, the magnitudes of contributions of individual orbits are found to exhibit a remarkable deformation dependence. Namely, Fourier peak heights associated with new orbits created by bifurcations quickly increase with increasing deformation and reach maximal values. Then, they start to decline. This behavior is seen in Fig. 6. Figure 8 displays the deformation dependence of the Fourier amplitudes $|F(L)|$ defined in Eq. (3·4) at lengths $L = L_\tau$ for some classical periodic orbits, which confirms the behavior noted above. This behavior has not been pointed out in the previous papers. It should be emphasized that the relative magnitudes and the deformation dependence of contributions of individual periodic orbits found here are significantly different from those roughly estimated in Ref. 9).

To get a deeper understanding of the mechanism of the enhancements associated with the bifurcations noted above, a semiclassical approximation that goes beyond the stationary phase approximation used in deriving the trace formula (3·2) may

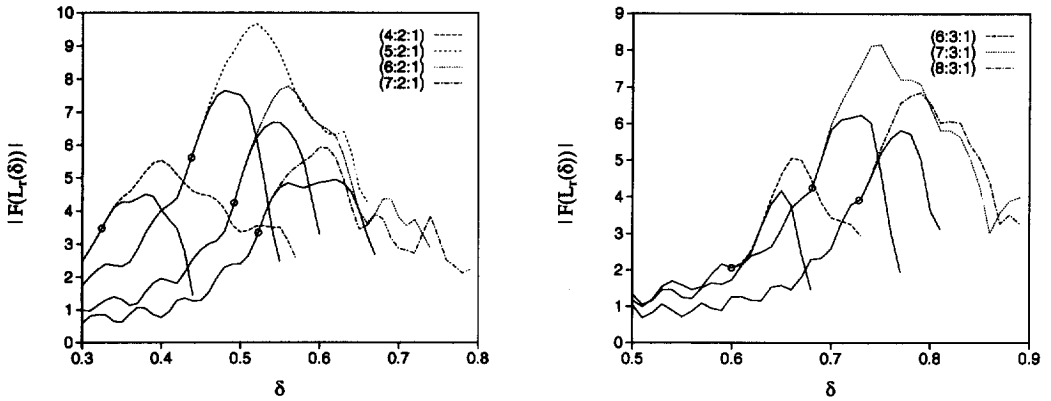

Fig. 8. Same as Fig. 5 but for meridian-plane hyperbolic orbits and 3D orbits (p:2:1) (left-hand side) and (p:3:1) (right-hand side). Solid curves correspond to those for equatorial-plane orbits from which these orbits are bifurcated.

be required. Such a semiclassical theory applicable for three dimensional deformed cavities is not available at present and remains a challenging subject for future study.

§7. Prolate hyperdeformations

Figure 9 displays Fourier transforms for $\delta = 0.7$ and 0.8. For $\delta \simeq 0.7$, the

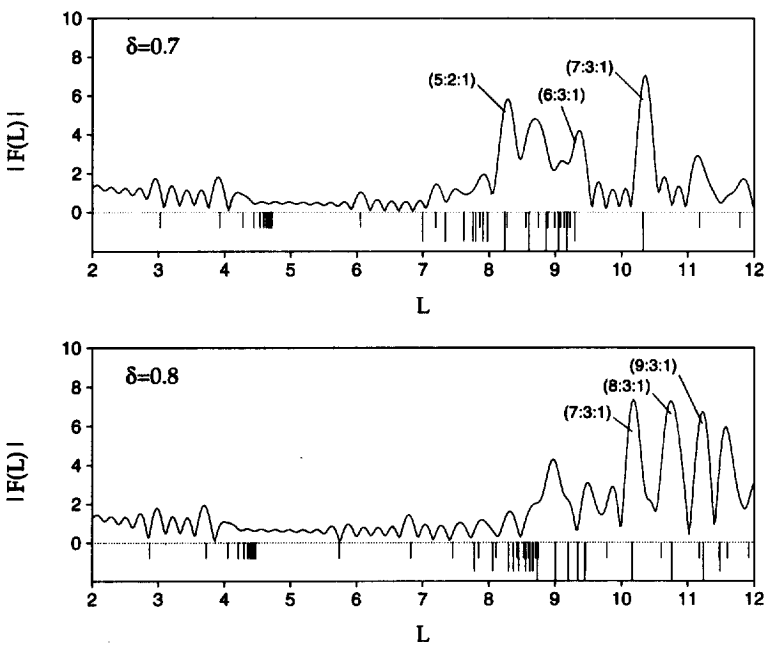

Fig. 9. Same as Fig. 6 but for $\delta = 0.7$ and 0.8 (axis ratio $\eta \simeq 2.3$ and 2.7).

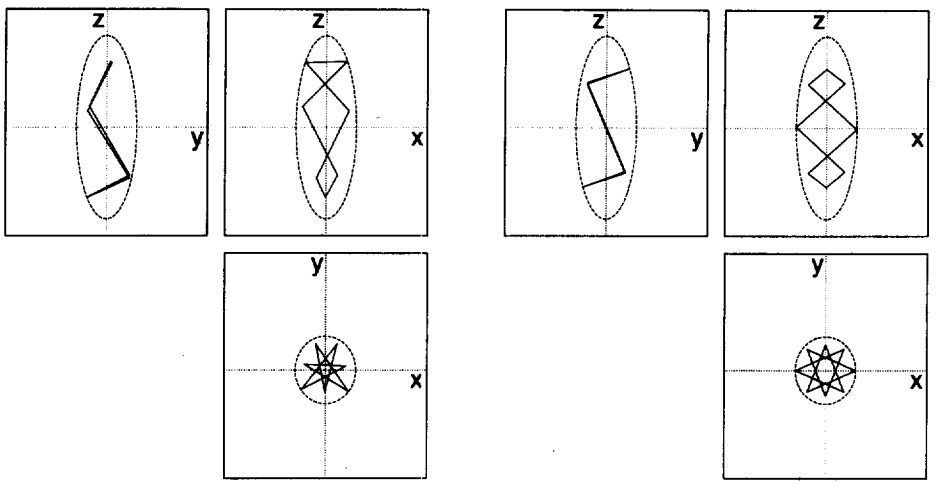

Fig. 10. Same as Fig. 7 but for 3D orbits (7:3:1) and (8:3:1) in the hyperdeformed prolate cavity with deformation $\delta = 0.8$.

peak at $L \simeq 10.3$ is associated with 3D orbits (7:3:1) bifurcated from 7-point star-shaped orbits in the equatorial plane. For $\delta = 0.80$, we see a rise of the peak at $L \simeq 10.8$, which is associated with 3D orbits (8:3:1) bifurcated from 8-point star-shaped orbits in the equatorial plane. They are displayed in Fig. 10. These 3D orbits resemble the Lissajous figures of the hyperdeformed harmonic oscillator with frequency ratio $\omega_\perp{:}\omega_z = 3{:}1$. In the same manner as for the 3D orbits responsible for superdeformations, Fourier peak heights associated with these newly appearing orbits rapidly increase after the bifurcations, reach the maxima and then decline with increasing deformation (see Fig. 8). Thus, also in this case, bifurcations of equatorial orbits (but of different types (p:3:1)) play the major role in the formation of this shell structure.

§8. Oblate superdeformations

Finally let us consider oblate deformations. Figure 11 displays Fourier transforms of quantum spectra for oblate spheroidal cavities with $\delta = -0.3 \sim -0.85$. For $\delta = -0.3$, the two dominant peaks are associated with triangular and tetragonal orbits in the meridian plane. For $\delta = -0.4$, we see a dominant peak at $L \simeq 6.3$ in addition to the peaks associated with the meridian-plane orbits. This new peak is associated with the butterfly-shaped planar orbits (4:1:1) bifurcated from double repetitions of linear orbits along the minor axis.

At $\delta = -0.75$ (axis ratio $\eta = 2$), the other peak at $L \simeq 7.5$ becomes important. This peak is associated with the triple traversals of linear orbits along the minor axis, which bifurcate just at this shape to planer hyperbolic orbits (6:1:1). They make a predominant contribution for $\delta = -0.85$ (peak at $L \simeq 7.1$).

Constant-action lines for these bifurcated orbits (4:1:1) and (6:1:1) are indicated in Figs. 2 and 3. We see clear correspondence between the shapes of these lines and

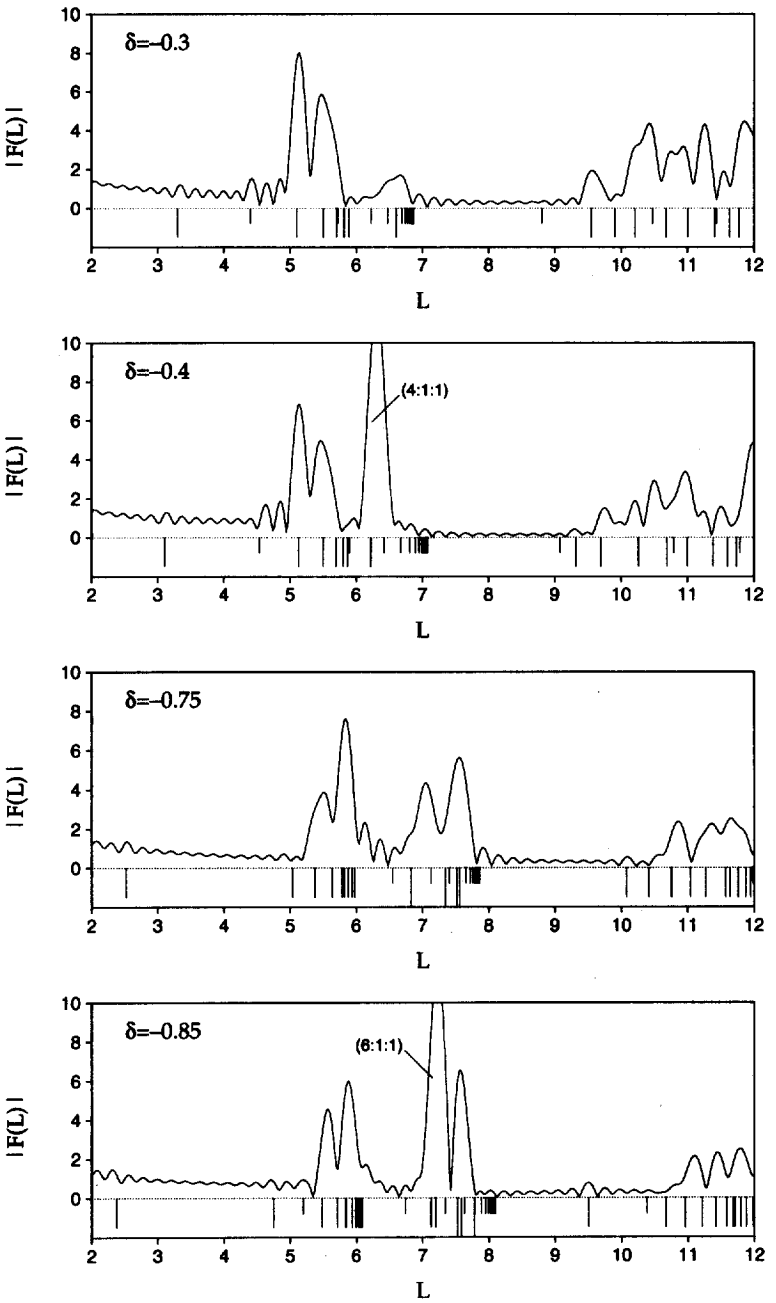

Fig. 11. Same as Fig. 6 but for oblate cavities with $\delta = -0.3 \sim -0.85$.

the shape of valleys in the oscillating level density. Combining this good correspondence with the behavior of the Fourier peaks mentioned above, it is evident that these periodic orbits are responsible for the shell structure at oblate superdeformations with an axis ratio of approximately 2:1. According to the classification given

in § 4, these are W-mode orbits.

In contrast to W-mode orbits, B-mode 3D orbits do not seem very important, although those with $(p{:}t{:}q) = (5{:}1{:}2), (6{:}1{:}2), \cdots$ etc. are already bifurcated from equatorial-plane orbits in the superdeformed region. This is an important difference between the prolate and the oblate superdeformations in the spheroidal cavity model.

§9. Conclusions

Classical periodic orbits responsible for the emergence of the superdeformed shell structure for single-particle motion in spheroidal cavities were identified and their relative contributions to the shell structures were evaluated. Both prolate and oblate superdeformations as well as prolate hyperdeformations were investigated.

Fourier transforms of quantum spectra clearly show that 3D periodic orbits born out of bifurcations of planar orbits in the equatorial plane become predominant at large prolate deformations, while butterfly-shaped planar orbits bifurcated from linear orbits along the minor axis are important at large oblate deformations.

Good correspondence between constant-action lines for these periodic orbits and valley structures in the oscillating part of the smoothed level density confirms the above conclusions.

After writing this paper, we learned that Magner et al.[20] carried out an extensive semiclassical analysis of shell structure in large prolate cavities. In their work, a rather large coarse-graining parameter γ for the level density was used, so that the equatorial-orbit bifurcations discussed in this paper were not clearly seen. It remains a challenge for future study to develop a semiclassical theory capable of treating equatorial-orbit bifurcations, and the phase-space trace formula proposed in Ref. 20) seems to provide a general framework for this aim.

Acknowledgements

We thank Matthias Brack, Alexander Magner, Zhang Xizhen, Rashid Nazmitdinov and Masayuki Matsuo for stimulating conversations.

References

1) P. J. Nolan and P. J. Twin, Ann. Rev. Nucl. Part. Sci. **38** (1988), 533.
2) R. V. F. Janssens and T. L. Khoo, Ann. Rev. Nucl. Part. Sci. **41** (1991), 321.
3) *Proceedings of the Workshop on Gammasphere Physics*, ed. M. A. Deleplanque, I. Y. Lee and A. O. Macchiavelli (World Scientific, 1996).
4) S. Åberg, H. Flocard and W. Nazarewicz, Ann. Rev. Nucl. Part. Sci. **40** (1990), 439.
5) M. C. Gutzwiller, J. Math. Phys. **12** (1971), 343.
6) R. Balian and C. Bloch, Ann. of Phys. **69** (1972), 76.
7) M. V. Berry and M. Tabor, Proc. R. Soc. London **A349** (1976), 101.
8) M. Brack and R. K. Bhaduri, *Semiclassical Physics* (Addison-Wesley, Reading, 1997).
9) V. M. Strutinsky, A. G. Magner, S. R. Ofengenden and T. Døssing, Z. Phys. **A283** (1977), 269.
10) R. Arvieu, F. Brut, J. Carbonell and J. Touchard, Phys. Rev. **A35** (1987), 2389.
11) Y. Ayant and R. Arvieu, J. of Phys. **A20** (1987), 397.
12) R. Arvieu and Y. Ayant, J. of Phys. **A20** (1987), 1115.
13) H. Frisk, Nucl. Phys. **A511** (1990), 309.

14) H. Nishioka, M. Ohta and S. Okai, Mem. Konan Univ. Sci. Ser. **38**(2) (1991), 1.
15) H. Nishioka, N. Nitanda, M. Ohta and S. Okai, Mem. Konan Univ. Sci. Ser. **39**(2) (1992), 67.
16) K. Arita, A. Sugita and K. Matsuyanagi, *Proc. Int. Symp. on Similarities and Differences between Nuclei and Clusters*, Tsukuba, July 1–4, 1997, AIP Conference Proceedings 416, ed. Y. Abe, I. Arai, S. M. Lee and K. Yabana, p. 393.
Proc. Int. Symp. on Atomic Nuclei and Metallic Clusters: Finite Many-Fermion Systems, Prague, Sep. 1–5, 1997, Czech. J. of Phys. **48** (1998), 821.
Proc. Int. Conf. on Nuclear Structure and Related Topics, Dubna, Sep. 9–13, 1997 (Joint Institute for Nuclear Research, 1997), ed. S. N. Ershov, R. V. Jolos and V. V. Voronov, p. 198.
17) T. Mukhopadhyay and S. Pal, Nucl. Phys. **A592** (1995), 291.
18) A. Sugita, K. Arita and K. Matsuyanagi, Prog. Theor. Phys. **100** (1998), 597.
19) H. Nishioka, Klavs Hansen and B. R. Mottelson, Phys. Rev. **B42** (1990), 9377.
20) A. G. Magner, S. N. Fedotkin, F. A. Ivanyuk, P. Meier, M. Brack, S. M. Reimann and H. Koizumi, Ann. der Phys. **6** (1997), 555.
See also A. G. Magner, S. N. Fedotkin, F. A. Ivanyuk, P. Meier and M. Brack, *Proc. Int. Conf. on Atomic Nuclei and Metallic Clusters: Finite Many-Fermion Systems*, Prague, Sep. 1–5, 1997, Czech. J. of Phys. **48** (1998), 845.